ity and stimulates translation via the interaction of poly(A) binding protein (PABP) with the 5′ m7G cap (*28*–*30*). Previous studies have found that miRNAs inhibit Cap-dependent translation (*33*) and induce mRNA degradation (*19*, *22*, *23*, *34*). We therefore postulate that miRNA-induced deadenylation is one of the mechanisms by which miRNAs enhance target decay and repress productive translation (fig. S12). Although it remains to be determined whether deadenylation is the primary step in mRNA regulation, we observed that block of translation does not accelerate mRNA deadenylation to the same extent as the miRNA does. It is therefore conceivable that miRNAs induce the deadenylation of their targets, which results in the block of translation and the recruitment to processing bodies (P-bodies), where mRNAs are decapped and degraded (*33*–*38*). Taken together, our results suggest that miRNAs promote the deadenylation and decay of hundreds of target mRNAs and thus sharpen and accelerate the transition between developmental states.

References and Notes

1. D. P. Bartel, *Cell* **116**, 281 (2004).
2. I. Alvarez-Garcia, E. A. Miska, *Development* **132**, 4653 (2005).
3. A. J. Giraldez *et al.*, *Science* **308**, 833 (2005); published online 17 March 2005 (10.1126/science.1109020).
4. B. D. Harfe, M. T. McManus, J. H. Mansfield, E. Hornstein, C. J. Tabin, *Proc. Natl. Acad. Sci. U.S.A.* **102**, 10898 (2005).
5. R. C. Lee, R. L. Feinbaum, V. Ambros, *Cell* **75**, 843 (1993).
6. B. J. Reinhart *et al.*, *Nature* **403**, 901 (2000).
7. E. C. Lai, *Genome Biol.* **5**, 115 (2004).
8. B. Wightman, I. Ha, G. Ruvkun, *Cell* **75**, 855 (1993).
9. H. Grosshans, T. Johnson, K. L. Reinert, M. Gerstein, F. J. Slack, *Dev. Cell* **8**, 321 (2005).
10. R. J. Johnston, O. Hobert, *Nature* **426**, 845 (2003).
11. A. Stark, J. Brennecke, R. B. Russell, S. M. Cohen, *PLoS Biol.* **1**, E60 (2003).
12. A. J. Enright *et al.*, *Genome Biol.* **5**, R1 (2003).
13. B. John *et al.*, *PLoS Biol.* **2**, e363 (2004).
14. B. P. Lewis, C. B. Burge, D. P. Bartel, *Cell* **120**, 15 (2005).
15. B. P. Lewis, I. H. Shih, M. W. Jones-Rhoades, D. P. Bartel, C. B. Burge, *Cell* **115**, 787 (2003).
16. A. Krek *et al.*, *Nat. Genet.* **37**, 495 (2005).
17. A. Stark, J. Brennecke, N. Bushati, R. B. Russell, S. M. Cohen, *Cell* **123**, 1133 (2005).
18. K. K.-H. Farh *et al.*, *Science* **310**, 1817 (2005); published online 22 November 2005 (10.1126/science.1121158).
19. L. P. Lim *et al.*, *Nature* **433**, 769 (2005).
20. P. Y. Chen *et al.*, *Genes Dev.* **19**, 1288 (2005).
21. J. Newport, M. Kirschner, *Cell* **30**, 687 (1982).
22. S. Bagga *et al.*, *Cell* **122**, 553 (2005).
23. Q. Jing *et al.*, *Cell* **120**, 623 (2005).
24. E. C. Lai, *Nat. Genet.* **30**, 363 (2002).
25. J. G. Doench, P. A. Sharp, *Genes Dev.* **18**, 504 (2004).
26. J. Brennecke, A. Stark, R. B. Russell, S. M. Cohen, *PLoS Biol.* **3**, e85 (2005).
27. S. Mathavan *et al.*, *PLoS Genet.* **1**, 260 (2005).
28. J. D. Richter, *Microbiol. Mol. Biol. Rev.* **63**, 446 (1999).
29. S. Vasudevan, E. Seli, J. A. Steitz, *Genes Dev.* **20**, 138 (2006).
30. C. H. de Moor, H. Meijer, S. Lissenden, *Semin. Cell Dev. Biol.* **16**, 49 (2005).
31. J. Krutzfeldt *et al.*, *Nature* **438**, 685 (2005).
32. M. W. Rhoades *et al.*, *Cell* **110**, 513 (2002).
33. R. S. Pillai *et al.*, *Science* **309**, 1573 (2005); published online 4 August 2005 (10.1126/science.1115079).
34. R. S. Pillai, *RNA* **11**, 1753 (2005).
35. J. Liu, M. A. Valencia-Sanchez, G. J. Hannon, R. Parker, *Nat. Cell Biol.* **7**, 719 (2005).
36. L. Ding, A. Spencer, K. Morita, M. Han, *Mol. Cell* **19**, 437 (2005).
37. J. Liu *et al.*, *Nat. Cell Biol.* **7**, 1161 (2005).
38. J. Rehwinkel, I. Behm-Ansmant, D. Gatfield, E. Izaurralde, *RNA* **11**, 1640 (2005).
39. F. J. Salles, W. G. Richards, S. Strickland, *Methods* **17**, 38 (1999).

40. We thank C. Antonio, I. Baptista, V. Greco, H. Knaut, H. Lopez-Schier, S. Mango, T. Schell, and W. Talbot for providing helpful comments on the manuscript. A.J.G. was supported by European Molecular Biology Organisation and is currently supported by a Human Frontier Science Program fellowship. A.F.S. was an Irma T. Hirschl Trust Career Scientist and an Established Investigator of the American Heart Association. This work was also supported by grants from the NIH (A.F.S.). Array data has been deposited in Gene Expression Omnibus (GEO) database under accession number GSE4201.

Supporting Online Material

www.sciencemag.org/cgi/content/full/1122689/DC1
Materials and Methods
Figs. S1 to S12
Table S1(≥1.5fold).xls
Targets-tested.doc

16 November 2005; accepted 8 February 2006
Published online 16 February 2006;
10.1126/science.1122689
Include this information when citing this paper.

Evolution of the Eastern Tropical Pacific Through Plio-Pleistocene Glaciation

Kira T. Lawrence,* Zhonghui Liu, Timothy D. Herbert

A tropical Pacific climate state resembling that of a permanent El Niño is hypothesized to have ended as a result of a reorganization of the ocean heat budget ~3 million years ago, a time when large ice sheets appeared in the high latitudes of the Northern Hemisphere. We report a high-resolution alkenone reconstruction of conditions in the heart of the eastern equatorial Pacific (EEP) cold tongue that reflects the combined influences of changes in the equatorial thermocline, the properties of the thermocline's source waters, atmospheric greenhouse gas content, and orbital variations on sea surface temperature (SST) and biological productivity over the past 5 million years. Our data indicate that the intensification of Northern Hemisphere glaciation ~3 million years ago did not interrupt an almost monotonic cooling of the EEP during the Plio-Pleistocene. SST and productivity in the eastern tropical Pacific varied in phase with global ice volume changes at a dominant 41,000-year (obliquity) frequency throughout this time. Changes in the Southern Hemisphere most likely modulated most of the changes observed.

A notable inflection point in the global benthic oxygen isotope ($\delta^{18}O$) record at ~3 million years ago (Ma) marks the beginning of the Plio-Pleistocene transition (*1*). During the preceding early Pliocene interval (3 to 5.3 Ma), there was little or no ice in the Northern Hemisphere (*2*), and global mean surface temperatures were ~3°C warmer than they are today (*3*). However, at ~3 Ma, benthic $\delta^{18}O$ values and ice-rafted debris in the North Atlantic and North Pacific signal two substantial changes in high-latitude climate (*4*–*6*). The Northern Hemisphere began a period of long-term growth in continental ice, most rapidly between about 3 and 2 Ma. At the same time, the variability of high-latitude climate increased markedly, as seen by the growing amplitude of 41,000-year (41-ky) obliquity cycles in benthic $\delta^{18}O$ beginning ~3 Ma (*7*). What was the manifestation of this climatic transition in the tropics? One emerging theory is that the tropical ocean shifted from a state much like permanent El Niño before ~3 Ma to its modern, more La Niña–like state after ~3 Ma (*8*–*11*).

In the modern ocean, the ventilated thermocline (the strong vertical thermal gradient between warm surface waters and cool deep waters) in the EEP brings cold, nutrient-rich waters to the surface, which are initially derived from the sinking of mid- to high-latitude surface waters in the Southern and Northern hemispheres (*9*, *12*–*14*). This outcropping of cold, nutrient-rich water gives rise to high productivity in the EEP and sets up east-west SST and atmospheric pressure gradients, which reinforce and are reinforced by the Trade Winds. At present, mean annual SSTs are 23°C in the EEP and 29°C in the western equatorial Pacific (WEP), yielding a modern surface temperature difference of 6°C (*15*). The resulting temperature gradient and associated pressure gradients drive the strong east-west atmospheric circulation pattern (Walker Circulation). A disruption of Walker Circulation gives rise to El Niño conditions, in which weaker easterly Trade Winds and a deeper thermocline in the EEP result in a warming of surface waters and a concomitant decline in biological productivity.

A recent theory (*9*) connects the posited transition from a permanent El Niño to a La Niña climate state to a fundamental change in linkages between the high- and low-latitude ocean on long-term time scales (>10^6 years) and orbital time scales (10^4 to 10^5 years). According to this

Department of Geological Sciences, Brown University, Box 1846, Providence, RI 02912, USA.

*To whom correspondence should be addressed. E-mail: kira_lawrence@brown.edu

theory, the gradual cooling of the deep ocean culminated ~3 Ma in a shoaling of the ventilated thermocline and gave rise for the first time to cold tropical upwelling zones, ending the permanent El Niño. In this new La Niña–like state, low- and high-latitude climates became linked because heat gained in low-latitude upwelling zones must be balanced by heat lost to the atmosphere at high latitudes. According to the Philander and Fedorov (*9*) theory, one manifestation of the end of the permanent El Niño configuration should be the appearance of 41-ky obliquity cycles in tropical upwelling zones. High obliquity would result in deglaciated high latitudes and El Niño–like conditions in the tropical Pacific (i.e., a deeper EEP thermocline), which should correspond to warmer and less productive conditions in the EEP. In contrast, low obliquity would induce glaciation and La Niña–like conditions (i.e., a shallower EEP thermocline), which should correspond to observations of a colder, more productive EEP.

Here, we test the hypotheses that the EEP upwelling zone and the low-latitude obliquity response arose synchronously during the late Pliocene (~3 Ma). Using the alkenone unsaturation index ($U^{k'}_{37}$)—a faithful recorder of mean annual SST (*16*, *17*) and changes in alkenone concentration (C_{37} Total), which is a proxy for phytoplankton productivity (*18*, *19*)—we monitored the evolution of two defining characteristics of the modern EEP: its cool SST and high biological productivity. Our data set from Ocean Drilling Program (ODP) Site 846 (3°S, 91°W; water depth 3296 m) is 5 million years (My) long and provides the longest high-resolution (~3-ky) record of Earth surface temperatures extant. This record allows us to evaluate linkages between different aspects of the Earth's climate system on both orbital time scales (10^4 to 10^5 years) and supra-orbital time scales (>10^6 years). Our results show that obliquity has modulated EEP surface conditions for at least the past 5 My. However, the EEP obliquity response increased substantially starting ~3 Ma as the EEP upwelling zone cooled and the SST gradient between the eastern and western Pacific grew.

EEP surface ocean variations. The Site 846 $U^{k'}_{37}$ SST record documents a long-term cooling of ~1°C/My with temperatures as high as 28°C in the early Pliocene and as low as 20°C in the late Pleistocene (Fig. 1B). Average SST at Site 846 (26°C) during the early Pliocene (3 to 5 Ma) approached values typical of the region during modern El Niño events (~27°C). Much of the Site 846 SST record is notably similar in trend and structure to the Site 846 benthic $\delta^{18}O$ record (*20*, *21*) (Fig. 1), illustrating that substantial Plio-Pleistocene cooling extended into the tropics. Similar to the benthic $\delta^{18}O$ record, SST variations increased in amplitude ~3 Ma (Fig. 1, B and C). Low-amplitude glacial-interglacial temperature cycles (average amplitude ~1°C) dominate the early Pliocene (3 to 5 Ma) SST record. Amplitudes increased during the late Pliocene with variations as large as 5°C (Fig. 1B). In contrast to the benthic $\delta^{18}O$, in which the major inflection point occurs at ~3 Ma and corresponds to substantial ice growth or high-latitude cooling, the $U^{k'}_{37}$ SST record shows that important changes happened before ~3 Ma (Fig. 1, B and C). Cooling in the surface ocean of the EEP started at least 1 My before the intensification of Northern Hemisphere glaciation (NHG), implying that while the growth of Northern Hemisphere ice sheets undoubtedly played a major role as a climatic feedback during the Plio-Pleistocene transition, it did not force or initiate EEP cooling (Fig. 1, B and C).

Our results from the EEP confirm the results of Wara *et al*. (*11*) (who found much warmer, more El Niño–like conditions, in the EEP based on Mg/Ca paleothermometry) and refute the conclusion of Rickaby and Halloran (*22*) (who found that conditions in the tropical Pacific during the Pliocene were cool and La Niña–like). However, our orbitally resolved SST time series shows that Site 846 SST estimates are an average of ~2°C cooler than those of Wara *et al*. (*11*) at Site 847 and suggests that EEP cooling began not at ~2.5 Ma, as suggested by Wara *et al*. (*11*), but at least as early as 4.3 Ma (Fig. 1B). These discrepancies may stem from actual differences in the dynamics between study sites several hundred kilometers apart in the EEP, from changes and differences in the ecology of the species responsible for the paleoclimate indexes measured (haptophyte algae for the $U^{k'}_{37}$ index versus the planktonic foraminifer *Globigerinoides sacculifer* for the Mg/Ca proxy) (*23*), from differences between the calibrations for alkenone and Mg/Ca paleothermometry, or from aliasing of orbital-scale variability in the Wara *et al*. (*11*) record, which has lower resolution.

Overall, high alkenone fluxes in sediments from ODP Site 846 [average mass accumulation rates (MAR) of 61 μg/cm²/ky] in comparison to alkenone MARs reported from other oceanic locations (0.1 to 35 μg/cm²/ky) (*18*, *24*) suggest that the EEP has been a locus of high biological productivity for at least the past 5 My. Alkenone concentration variations highlight a regime between 2.9 and 1.6 Ma of distinctly higher productivity than came before or after [Fig. 1A, supporting online material (SOM) text, and fig. S1]. Alkenone concentrations during this interval were three times and two times as high as average early Pliocene and Pleistocene values, respectively. This finding is corroborated by a similar maximum in the MAR of biogenic carbonate in the subtropical eastern Pacific between 2.9 and 1.7 Ma (*8*). On glacial-interglacial time scales, higher alkenone concentrations almost universally occur during cold intervals (Fig. 1, A and B), indicating that temperature and productivity were tightly coupled on orbital time scales (≤10^5 years). Increased variance in both the SST and $\delta^{18}O$ records (Fig. 2, A and B) accompanies the marked increase in productivity at ~2.9 Ma (Fig. 1A). The de-

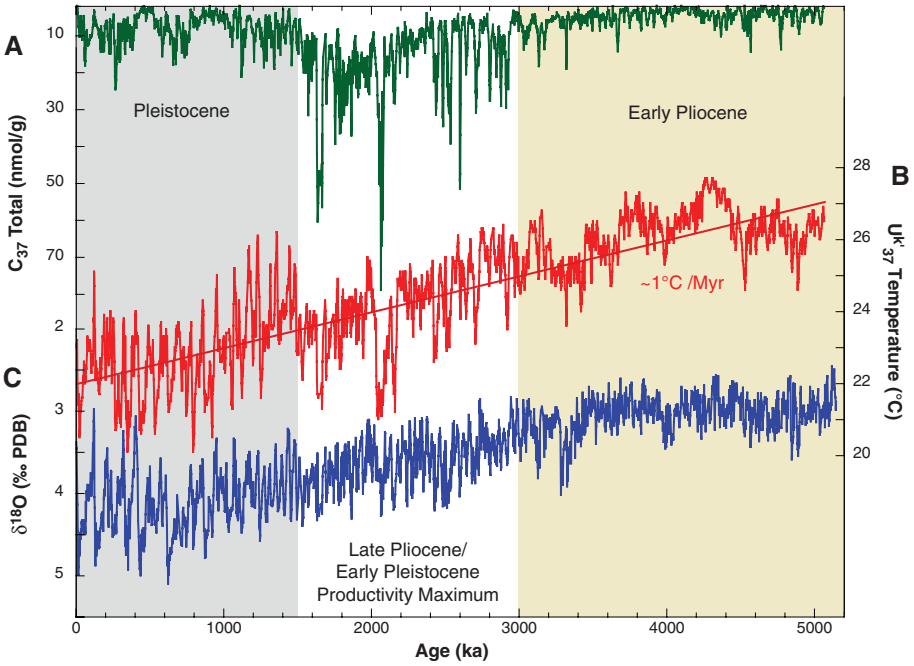

Fig. 1. Paleoclimatic proxies from ODP Site 846. (**A**) Concentration of C_{37} alkenones (nmol/g) (green line) (note the inverted axis), (**B**) $U^{k'}_{37}$ sea surface temperature (°C) (red line), and (**C**) benthic $\delta^{18}O$ in parts per thousand PD belemnite (PDB) (note the inverted axis) (*20*, *21*). All data are correlated to the LR04 Stack (*7*) with the use of the Match 2.0 program (*32*). The early Pliocene is shaded yellow, a white background defines the interval of maximum EEP productivity, and the portion of the Pleistocene after the productivity maximum is shaded gray. ka, thousands of years ago.

cline in productivity at ~1.6 Ma corresponds to a slight warming of SST (~1°C) during the interval from 1.6 to 1 Ma (Fig. 1, A and B).

Evolutionary spectra of Site 846 $\delta^{18}O$, $U^{k'}_{37}$ temperature, and C_{37} Total show that obliquity power plays a dominant role in all three records over the past 5 My (Fig. 2, A to C). The 1.2-My modulation (i.e., the envelope of the obliquity signal), notable in the orbital forcing as a series of alternating intervals of strong versus weak spectral density (Fig. 2D), is discernable in all three climatic responses (Fig. 2, A to C). Similar to $\delta^{18}O$, the $U^{k'}_{37}$ SST record shows a pronounced increase in obliquity band variance toward the present, starting at ~3 Ma (Fig. 2, A and B). In contrast, the C_{37} Total productivity record responds more faithfully to obliquity pacing, with a strong response at 41 ky observed even before the intensification of NHG (~3 Ma) (Fig. 2C).

In the obliquity band, all three proxies are coherent for the majority of the past 5 My (Fig. 3, A to C). The exceptions generally coincide with obliquity nodes (intervals of low obliquity amplitude) when obliquity band climatic forcing is weak (Fig. 3D). SST and C_{37} Total are anticorrelated (cold temperatures correspond to high productivity) throughout the entire interval, as shown by the nearly constant phase relationship –1 ± 1.5 ky (±2σ) between SST and C_{37} Total (Fig. 3A). After ~2.5 Ma, both temperature and C_{37} Total slightly lead (3 ± 1.5 ky and 4 ± 1.75 ky, respectively) benthic $\delta^{18}O$ in the obliquity band (Fig. 3, B and C, and SOM text). Before this time, all proxies are more nearly in phase (Fig. 3, B and C). The slight increase in lag of benthic $\delta^{18}O$ relative to changes in sea surface indices after 2.5 Ma may testify to the greater thermal inertia of Northern Hemisphere ice sheets as they rapidly expanded during the intensification of NHG (*25*).

Mechanisms for EEP sea surface change. What mechanisms gave rise to these orbital-scale and longer term climatic variations in the EEP sea surface? Plausible mechanisms for altering EEP SST are changing (i) local insolation, (ii) the east-west tilt of the thermocline, (iii) the average depth of the thermocline, or (iv) the composition of the atmosphere (i.e., changing greenhouse gas concentrations). EEP productivity could be changed by altering (i) the east-west tilt of the thermocline, (ii) the average depth of the thermocline, or (iii) the nutrient content of the source waters. Some of these mechanisms result in coupled changes in SST and productivity. Others may lead to independent changes in one proxy record without a corresponding change in the other. For example, changing the depth or tilt of the thermocline should result in changes in both SST and productivity, whereas changes in atmospheric composition can affect ocean surface temperature without modifying biological productivity. However, these mechanisms are not necessarily mutually exclusive. The ODP Site 846 record suggests that temperature and productivity of the eastern Pacific upwelling zone were tightly coupled on orbital time scales, but only weakly coupled on long time scales, implying that different mechanisms may drive changes in EEP surface conditions on these two time scales.

Orbital time scales. At low latitudes, changes in seasonal insolation caused by variations in precession [~10 watts per m^2 (Wm^{-2})] are far greater than those driven by obliquity oscillations (<1 Wm^{-2}), suggesting that important low-latitude climatic processes (such as Trade Winds and monsoons) should vary at precessional periods. However, our low-latitude sea surface records have only weak precessional power (Fig. 2, B and C), implying a marginal role for low-latitude processes in orbital-scale variations in EEP climate over the past 5 My. Instead, obliquity oscillations dominated EEP records of both productivity and temperature for most of this time and were nearly in phase (average lead of 2 to 3 ky) with changes in benthic $\delta^{18}O$ wherever the signals were coherent (Fig. 3, B and C). Although we cannot precisely measure the phase relationship of geological responses to orbital obliquity forcing, the unambiguous coupling of a colder and more productive EEP with enriched benthic $\delta^{18}O$ indirectly demonstrates a consistent link between low orbital obliquity, which favors ice sheet growth in high latitudes, and the cold EEP we document here (SOM text). As previously documented for the early Pleistocene (*26*), SST variations were out of phase with low-latitude obliquity insolation changes throughout the entire time series (i.e., the EEP cooled in a low orbital obliquity configuration, which actually provided more solar heating to the tropics).

The tight coupling between SST and productivity implies that high-latitude obliquity variations adjusted either the tilt or depth of the EEP thermocline. These relationships are consistent with the obliquity-related changes in thermocline depth predicted by Philander and Fedorov (*9*). When obliquity was high, EEP conditions were El Niño–like, with warm SSTs and low productivity, implying a deep mean depth of the thermocline; when obliquity was low, EEP conditions were La Niña–like, with cold SSTs and high productivity, implying a shallow mean depth of the thermocline.

The El Niño model might successfully account for SST and productivity changes observed

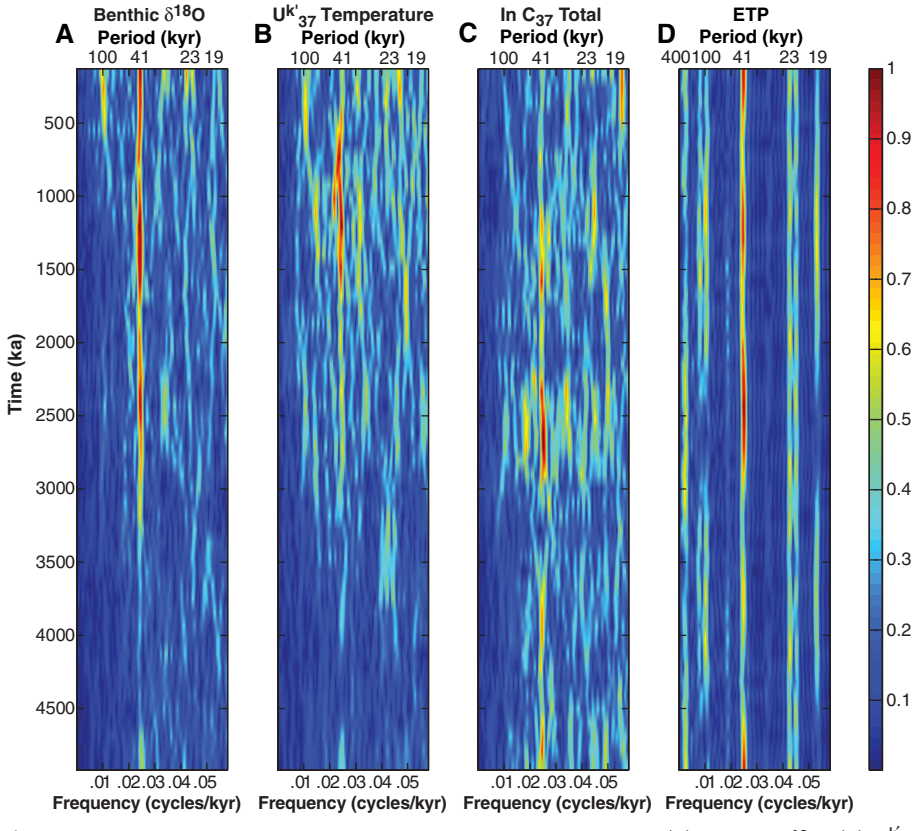

Fig. 2. Evolutionary spectra of ODP 846 paleoclimate proxies and ETP. (**A**) Benthic $\delta^{18}O$, (**B**) $U^{k'}_{37}$ temperature, and (**C**) natural logarithm (ln) C_{37} Total (alkenone concentration) (*18*, *19*). (**D**) Eccentricity, obliquity (tilt), and precession (ETP) (*33*). ETP is an illustration of changes in orbital variations through time. These spectra were computed with the use of a fast Fourier transform (FFT) with a 600-ky window and 85% overlap between windows. All responses were interpolated to even intervals of 1-ky resolution and prewhitened (except ETP) before being subjected to the FFT. The same major spectral features are reproducible with the use of the Blackman-Tukey method, indicating that the results produced in this analysis are not methodology dependent.

in the EEP considered in isolation, but recent SST estimates from the Pleistocene western Pacific suggest that the El Niño model incompletely describes the larger tropical Pacific on orbital time scales. Two recent studies have shown that during the early Pleistocene glacial-interglacial SST variations in the western equatorial Pacific were dominated by 41-ky cycles, with warmings and coolings of similar amplitude and phasing as those in the East (*27*, *28*) (fig. S2). In the modern ocean, El Niño results in a SST seesaw in the equatorial Pacific Ocean. One would therefore expect to find opposing SST responses between east and west in a pure El Niño model of 41-ky cyclicity. Instead, the similarity in glacial-interglacial phasing and amplitude of SSTs between the EEP and the WEP during the Pleistocene (fig. S2) implies the existence of a mechanism capable of synchronizing tropical SST changes in a manner not consistent with a simple vertical movement or rocking of the thermocline. We concur with Medina-Elizalde and Lea (*27*), who concluded that changing concentrations of atmospheric greenhouse gases were an important component of orbital-scale SST changes during the Pleistocene. We hypothesize that in addition to movements of the thermocline, greenhouse forcing likely played a major role in driving orbital-scale SST variability in the EEP throughout the past 5 My.

Long time scales. Despite the occurrence of major global climatic changes at ~3 Ma, which in the EEP were recorded as a marked increase in obliquity band variance of both $\delta^{18}O$ and EEP SST (Fig. 2, A and B) and a threefold increase in alkenone concentration (Fig. 1A), the obliquity band coherency and phase relationships between EEP SST, productivity, and $\delta^{18}O$ remained essentially unchanged (Fig. 3, A to C). If we accept benthic $\delta^{18}O$ as a high-latitude proxy, reflecting a combination of ice volume and deep-ocean temperature changes that are imparted at high latitudes, then the long-term constancy of these relationships suggests that the "plumbing" of the EEP upwelling system has not changed appreciably over the past 5 My and indicates that a strong link in the obliquity band existed between high- and low-latitude climates well before 3 Ma. The persistence of obliquity responses suggests that, consistent with the theory, but in contrast to the timing proposed by Philander and Fedorov (*9*), the high latitudes continued to modulate EEP surface conditions so long as a west-east SST gradient persisted (i.e., for at least the past 5 My) (fig. S3). Our results do not invalidate the fundamental tenet of the Philander and Fedorov (*9*) theory, which states that a major reorganization of the sources and sinks of the oceanic heat budget occurred in association with long-term cooling of the deep ocean, but they suggest that the onset of such a reorganization must be moved to before 5 Ma.

Given that Southern Hemisphere cooling and glaciation preceded that of the Northern Hemisphere by millions of years (*1*), we suggest that the critical establishment of a high- and low-latitude link by means of the thermocline may have depended more on oceanographic changes in the Southern, rather than Northern, Hemisphere. One of the most prominent observations implicating the role of the Southern Ocean in the evolution of EEP surface conditions is the poor correspondence of the high productivity interval between about 2.9 and 1.6 Ma (Fig. 1C) to either the local SST, as inferred from alkenone paleotemperatures, or to east-west equatorial Pacific gradients, as inferred from comparing our SST estimates at Site 846 with the (more sparsely sampled) Mg/Ca paleotemperature estimates from the Western Pacific Warm Pool (ODP Site 806) (*11*) (fig. S3). Substantial changes in EEP productivity occur in the modern El Niño Southern Oscillation cycle in response to shoaling or deepening of the equatorial thermocline and strengthening or weakening of the Trade Winds. An El Niño model would therefore predict that higher past productivity should coincide with colder EEP SST and enhanced east-west gradients. At the orbital scale, we do indeed observe the association of colder SST and higher past productivity. Yet, EEP productivity increased abruptly at 2.9 Ma without a similar anomaly of cold SST at Site 846, and the interval in which the west-east SST gradient became the strongest (past 1.5 My) (*8*, *11*) (fig. S3), counter to expectations, corresponds to a substantial decline in EEP surface productivity (Fig. 1A). Both of

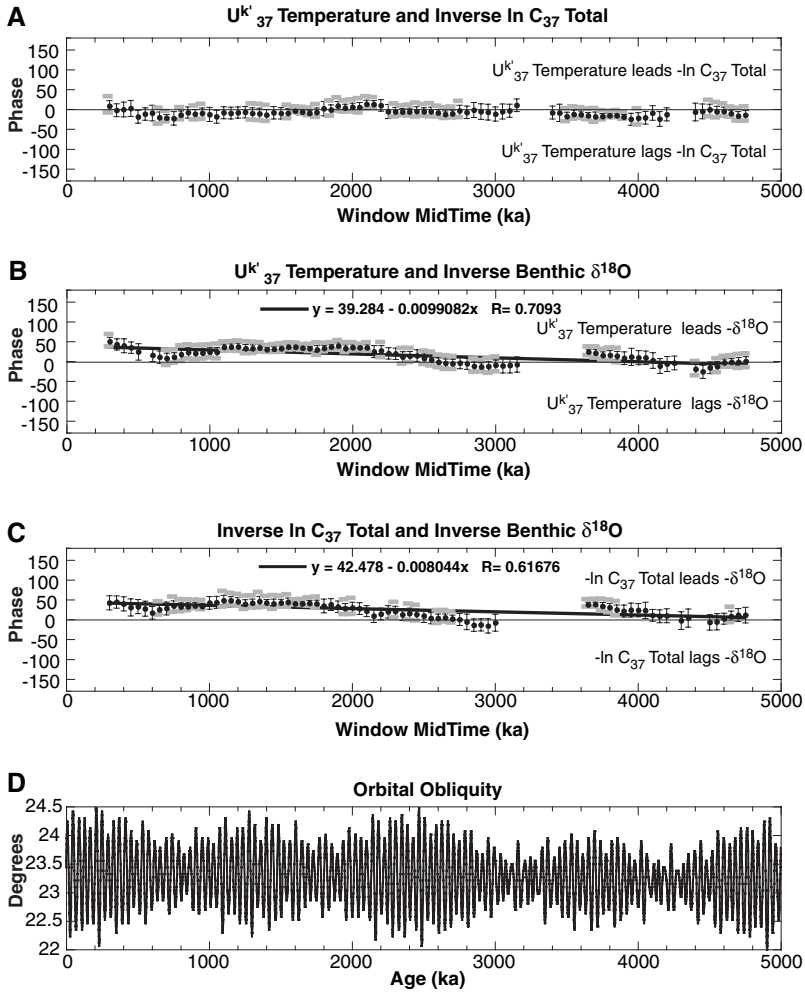

Fig. 3. Obliquity band (41-ky) phase and coherency relationships and orbital obliquity. (**A**) $U^{k'}_{37}$ temperature (SST) and alkenone concentration (productivity) (–ln C_{37} Total), (**B**) $U^{k'}_{37}$ temperature (SST) and benthic $-\delta^{18}O$ (ice volume), (**C**) alkenone concentration (productivity) (–ln C_{37} Total) and benthic $-\delta^{18}O$ (ice volume), and (**D**) orbital obliquity (*34*). Intervals that are coherent at the 80% confidence level are shown with thin black error bars and those that are coherent at the 95% confidence level are shown with thick gray bars. Because the alkenone concentrations have a log-normal rather than Gaussian distribution, we used the natural logarithm of alkenone concentration (C_{37} Total). We use the inverse of both benthic $\delta^{18}O$ and alkenone concentration in our coherency and phase analyses to be consistent with paleoclimatic convention and the axes in Fig. 1. Before coherency and phase analysis, all records were interpolated to even intervals of 1-ky resolution. Phases were computed with the use of the Arand Program iterative spectra feature with a 600-ky window and 300 lags. Regression lines [thick black lines in (B) and (C)] show the trend toward increasing phase difference toward the present.

these observations are inconsistent with a change in the tilt or depth of the thermocline uniquely determining the extent of EEP productivity.

We hypothesize that nutrient availability, a characteristic of the source waters, rather than a change in wind-driven upwelling strength, controlled productivity variations in the EEP on long time scales. Today, the cold, nutrient-rich waters of the ventilated thermocline that are upwelled in the EEP are sourced by intermediate and mode waters from the high latitudes of the North Pacific and the Southern Ocean (*12*, *14*), with greater contributions from the Southern Hemisphere (*13*). A crash in productivity in both of these high-latitude source regions occurred at approximately the same time as an abrupt increase in productivity in the EEP (Fig. 1A) and in the California margin upwelling zone (*8*), and in synchronicity with the major intensification of NHG (*29*, *30*). Recent studies suggest that polar stratification in the high-latitude source regions of EEP surface waters began at about 3 Ma (*29*, *30*). We hypothesize that nutrients that were not used at high latitudes after the intensification of NHG were instead entrained into the source waters for the EEP and fed the marked rise in productivity observed at Site 846 at ~3 Ma. The decline in productivity in the EEP between 1 and 2 Ma followed the establishment of the modern Southern Ocean opal belt at ~2 Ma (*31*), lending further support to the hypothesis that changes in nutrient availability of the source region drove major changes in EEP productivity. Given the large modern contribution of Southern Hemisphere waters to the EEP, the role that the high-latitude Southern Hemisphere climate played in the Plio-Pleistocene transition warrants more consideration.

References and Notes

1. J. Zachos, M. Pagani, L. C. Sloan, E. Thomas, K. Billups, *Science* **292**, 686 (2001).
2. A. M. Haywood, P. J. Valdes, B. W. Sellwood, *Global Planet. Change* **25**, 239 (2000).
3. A. M. Haywood, P. J. Valdes, *Earth Planet. Sci. Lett.* **218**, 363 (2004).
4. N. J. Shackleton *et al.*, *Nature* **307**, 620 (1984).
5. M. A. Maslin, G. H. Haug, M. Sarnthein, R. Tiedemann, *Geol. Rundsch.* **85**, 452 (1996).
6. H. Flesche Kleiven, E. Jansen, T. Fronval, T. M. Smith, *Palaeogeogr. Palaeoclimatol. Palaeoecol.* **184**, 213 (2002).
7. L. E. Lisiecki, M. E. Raymo, *Paleoceanography* **20**, PA1003 (2005).
8. A. C. Ravelo, D. H. Andreasen, M. Lyle, A. O. Lyle, M. W. Wara, *Nature* **429**, 263 (2004).
9. S. G. Philander, A. V. Fedorov, *Paleoceanography* **18**, 1045 (2003).
10. P. Molnar, M. A. Cane, *Paleoceanography* **17**, 1021 (2002).
11. M. W. Wara, A. C. Ravelo, M. L. Delaney, *Science* **309**, 758 (2005).
12. M. Tsuchiya, R. Lukas, R. A. Fine, *Prog. Oceanogr.* **23**, 101 (1989).
13. J. R. Toggweiler, K. Dixon, W. S. Broecker, *J. Geophys. Res.* **96**, 20467 (1991).
14. J. L. Sarmiento, N. Gruber, M. A. Brzezinski, J. P. Dunne, *Nature* **427**, 56 (2004).
15. S. Levitus, T. P. Boyer, *World Ocean Atlas* (NOAA Atlas NESDros. Inf. Serv., Washington, DC, 1994).
16. F. Prahl, L. A. Muehlhausen, D. L. Zahnle, *Geochemica et Cosmochimica Acta* **52**, 2303 (1988).
17. P. J. Müller, G. Kirst, G. Ruhland, I. von Storch, A. Rosell-Melé, *Geochim.Cosmochim. Acta* **62**, 1757 (1998).
18. D. Budziak *et al.*, *Paleoceanography* **15**, 307 (2000).
19. Materials and methods are available as supporting material on *Science* Online.
20. A. C. Mix, J. Le, N. J. Shackleton, *Proc. Ocean Drill. Program Sci. Res.* **138**, 839 (1995).
21. N. J. Shackleton, M. A. Hall, D. Pate, *Proc. Ocean Drill. Program Sci. Res.* **138**, 337 (1995).
22. R. E. M. Rickaby, P. Halloran, *Science* **307**, 1948 (2005).
23. H. J. Spero, K. M. Mielke, E. M. Kalve, D. W. Lea, D. K. Pak, *Paleoceanography* **18**, 1022 (2003).
24. M. A. Sicre, Y. Ternois, M. Paterne, P. Martinez, P. Bertrand, *Org. Geochem.* **32**, 981 (2001).
25. S. C. Clemens, D. W. Murray, W. L. Prell, *Science* **274**, 943 (1996).
26. Z. Liu, T. D. Herbert, *Nature* **427**, 720 (2004).
27. M. Medina-Elizalde, D. W. Lea, *Science* **310**, 1009 (2005).
28. T. de Garidel-Thoron, Y. Rosenthal, F. C. Bassinot, L. Beaufort, *Nature* **433**, 294 (2005).
29. D. M. Sigman, S. L. Jaccard, G. Haug, *Nature* **428**, 59 (2004).
30. G. H. Haug, D. M. Sigman, R. Tiedemann, T. F. Pedersen, M. Sarnthein, *Nature* **401**, 779 (1999).
31. G. Cortese, R. Gersonde, C.-D. Hillenbrand, G. Kuhn, *Earth Planet. Sci. Lett.* **224**, 509 (2004).
32. L. E. Lisiecki, P. A. Lisiecki, *Paleoceanography* **17**, 1049 (2002).
33. J. Imbrie *et al.*, in *Milankovitch and Climate, Part I*, A. Berger, Ed. (D. Reidel, Norwell, MA, 1984).
34. J. Laskar, F. Joulet, F. Boudin, *Astron. Geophys.* **270**, 522 (1993).

35. We acknowledge the Ocean Drilling Program (Texas A&M University) for supplying sediment samples. This work was supported by an Evolving Earth Foundation research grant (K.T.L.), by NSF through grant OCE-526372 (T.D.H.) and a graduate research fellowship (K.T.L.), and by the Geological Society of America through research grant #7447-03 (K.T.L.). We thank L. C. Cleaveland, L. Albertson, and L. Seckel for their help in laboratory analyses; L. Lisiecki for age model assistance; W. H. Hutson for time series analysis advice; and W. D'Andrea, C. Chazen, L. Lisiecki, A. C. Ravelo, and A. Fedorov for thoughtful suggestions. Data are available online (www.ncdc.noaa.gov/paleo/paleocean.html).

Supporting Online Material

www.sciencemag.org/cgi/content/full/312/5770/79/DC1
Materials and Methods
SOM Text
Figs. S1 to S3
References and Notes

20 September 2005; accepted 24 February 2006
10.1126/science.1120395

REPORTS

Generating Optical Schrödinger Kittens for Quantum Information Processing

Alexei Ourjoumtsev, Rosa Tualle-Brouri, Julien Laurat, Philippe Grangier*

We present a detailed experimental analysis of a free-propagating light pulse prepared in a "Schrödinger kitten" state, which is defined as a quantum superposition of "classical" coherent states with small amplitudes. This kitten state is generated by subtracting one photon from a squeezed vacuum beam, and it clearly presents a negative Wigner function. The predicted influence of the experimental parameters is in excellent agreement with the experimental results. The amplitude of the coherent states can be amplified to transform our "Schrödinger kittens" into bigger Schrödinger cats, providing an essential tool for quantum information processing.

A key requirement for many quantum computation and communication protocols (*1*, *2*) is to use specific quantum states of light as a resource for information processing. We are interested in quantum states of propagating light beams, which can be analyzed either by photon counting or by homodyne detection, which measures the interference between the signal state and an intense reference beam with a relative phase θ. Homodyne detection measures a physical quantity called a "quadrature component" of the electric field, associated with the operator $\hat{x}_\theta = \hat{x}\cos\theta + \hat{p}\sin\theta$, where $\hat{x}$ and $\hat{p}$ are canonically conjugate field observables. The operators $\hat{x}$ and $\hat{p}$ are analogous to the position and the momentum of a particle, and they are often called quantum continuous variables (QCVs). From Heisenberg's inequalities, they cannot be determined simultaneously with an infinite precision, so one cannot generally define a proper phase-space density $\Pi(x, p)$ for the electric field. However, one can define a quasi-distribution $W(x, p)$ called the Wigner function, the marginals of which yield the probability distributions $P(x_\theta)$. By measuring the distributions $P(x_\theta)$ for several values of θ, one can reconstruct the Wigner function; this inverse process is known as quantum tomography (*3*).

For specific quantum states, the Wigner function can take negative values, thereby excluding any description by a classical phase-space den-

Laboratoire Charles Fabry de l'Institut d'Optique, CNRS Unité Mixte de Recherche 8501, 91403 Orsay, France.

*To whom correspondence should be addressed. E-mail: philippe.grangier@iota.u-psud.fr